

Title Aluminum oxide/titanium dioxide nanolaminates grown by atomic layer deposition: Growth and mechanical properties

Author(s) Ylivaara, Oili M. E.; Kilpi, Lauri; Liu, Xuwen; Sintonen, Sakari; Ali, Saima; Laitinen, Mikko; Julin, Jaakko; Haimi, Eero; Sajavaara, Timo; Lipsanen, Harri; Hannula, Simo-Pekka; Ronkainen, Helena; Puurunen, Riikka L.

Citation Journal of Vacuum Science and Technology A. American Institute of Physics; American Vacuum Society. Vol. 35 (2017) No: 1 , 01B105, 14 pages

Date 2017

URL <http://dx.doi.org/10.1116/1.4966198>

Rights Accepted manuscript. This article may be downloaded for personal use only. Any other use requires prior permission of the author and AIP Publishing.

Self archived 8th December 2016

<p>VTT http://www.vtt.fi P.O. box 1000 FI-02044 VTT Finland</p>	<p>By using VTT Digital Open Access Repository you are bound by the following Terms & Conditions.</p> <p>I have read and I understand the following statement:</p> <p>This document is protected by copyright and other intellectual property rights, and duplication or sale of all or part of any of this document is not permitted, except duplication for research use or educational purposes in electronic or print form. You must obtain permission for any other use. Electronic or print copies may not be offered for sale.</p>
---	---

Aluminum oxide / titanium dioxide nanolaminates grown by atomic layer deposition: growth and mechanical properties

Running title: ALD Al₂O₃/TiO₂ nanolaminate growth and mechanical properties

Running Authors: Ylivaara et al.

Oili M. E. Ylivaara^{a)}

VTT Technical Research Centre of Finland, P.O.Box 1000, FI-02044 VTT, Finland

Lauri Kilpi

VTT Technical Research Centre of Finland, P.O.Box 1000, FI-02044 VTT, Finland

Xuwen Liu

Aalto University School of Chemical Technology, Department of Materials Science and Engineering, P.O.Box 16200, FI-00076 Aalto, Finland

Sakari Sintonen

Aalto University School of Electrical Engineering, Department of Micro- and Nanosciences, P.O.Box 13500, FI-00076 Aalto, Finland

Saima Ali

Aalto University School of Electrical Engineering, Department of Micro- and Nanosciences, P.O.Box 13500, FI-00076 Aalto, Finland

Mikko Laitinen

University of Jyväskylä, Department of Physics, P. O. Box 35, FI-40014 Jyväskylä, Finland

Jaakko Julin

University of Jyväskylä, Department of Physics, P. O. Box 35, FI-40014 Jyväskylä, Finland

Eero Haimi

Aalto University School of Chemical Technology, Department of Materials Science and Engineering, P.O.Box 16200, FI-00076 Aalto, Finland

Timo Sajavaara

University of Jyväskylä, Department of Physics, P. O. Box 35, FI-40014 Jyväskylä, Finland

Harri Lipsanen

Aalto University School of Electrical Engineering, Department of Micro- and Nanosciences, P.O.Box 13500, FI-00076 Aalto, Finland

Simo-Pekka Hannula

Aalto University School of Chemical Technology, Department of Materials Science and Engineering, P.O.Box 16200, FI-00076 Aalto, Finland

Helena Ronkainen

VTT Technical Research Centre of Finland, P.O.Box 1000, FI-02044 VTT, Finland

Riikka L. Puurunen

VTT Technical Research Centre of Finland, P.O.Box 1000, FI-02044 VTT, Finland

^{a)} Electronic mail: oili.ylivaara@vtt.fi

Atomic layer deposition (ALD) is based on self-limiting surface reactions. This and cyclic process enable the growth of conformal thin films with precise thickness control and sharp interfaces. A multi-layered thin film, that is nanolaminate, can be grown using ALD with tuneable electrical and optical properties to be exploited for example in the microelectromechanical systems. In this work the tunability of the residual stress, adhesion and mechanical properties of the ALD nanolaminates composed of aluminium oxide (Al_2O_3) and titanium dioxide (TiO_2) films on silicon were explored as a function of growth temperature (110 – 300 °C), film thickness (20 – 300 nm), bilayer thickness (0.1 – 100 nm) and TiO_2 content (0 – 100%). Al_2O_3 was grown from Me_3Al and H_2O , and TiO_2 from TiCl_4 and H_2O . According to wafer curvature measurements $\text{Al}_2\text{O}_3 / \text{TiO}_2$ nanolaminates were under tensile stress; bilayer thickness and growth temperature were the major parameters affecting the stress, the residual stress decreased with increasing bilayer thickness and ALD temperature. Hardness increased with increasing ALD temperature and decreased with increasing TiO_2 fraction. Contact modulus remained approximately stable. The adhesion of the nanolaminate film was good on silicon.

I. INTRODUCTION

Atomic layer deposition (ALD) is a thin film growth technique developed independently in the 1960s and 1970s under the names molecular layering and atomic layer epitaxy (ALE), respectively.^{1,2} ALD was industrialized in 1980s for thin-film electroluminescent (TFEL) displays and in 2000s for microelectronics such as dynamic random-access memories (DRAM) and complementary metal-oxide semiconductor (CMOS) transistors.^{1,2,3,4,5} ALD thin films can be grown with sub-monolayer thicknesses, since in each growth cycle self-limiting surface reactions take place.^{3,4,6} This unique feature enables precise thickness control and high conformality^{7,8} of the grown film by simply controlling the number of growth cycles.

Nanolaminates are multilayer films, engineered of at least two different materials.^{9,10} A typical nanolaminate structure, presented in Figure 1, is composed of repeated bilayers, each bilayer consisting of two materials with separately defined thicknesses. These individual sublayer thicknesses are determined by the number of ALD growth cycles. To reach the total nanolaminate thickness, the number of bilayers is repeated by a given number of the nanolaminate supercycles. A nanolaminate might also have optional bottom and top layer (a “cap”).

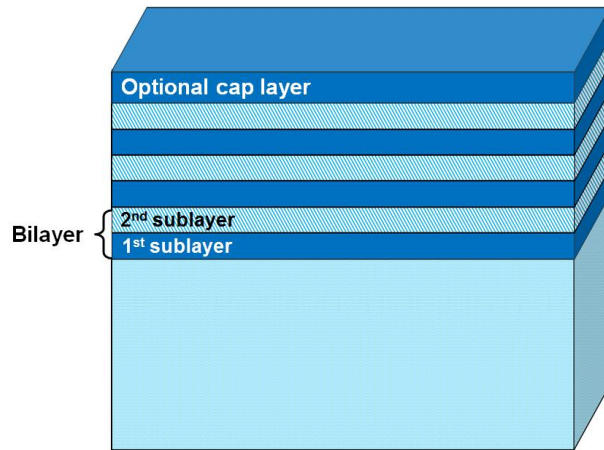


FIG. 1. (Color online) A schematic representation of a typical nanolaminate structure with three bilayers, and a cap layer.

The thickness control, multilayer processing capability, uniformity and conformality of the ALD^{10,11,12} are advantageous in processing nanolaminated thin films. With ALD, nanolaminates can be grown either with sharp interfaces^{13,14} or gradual composition changes.¹⁵ Thus the ALD enables engineering of the nanolaminates with tuneable physical properties,¹⁵ by choosing the layer thickness to be less or equal to the length scale that defines the physical property.^{6,15,16}

ALD nanolaminates were introduced in TFEL-displays,^{17,18} and optical dielectric multilayers.^{10,11} Especially $\text{Al}_2\text{O}_3 / \text{TiO}_2$ nanolaminates have applications in optics,^{10,19} because the Al_2O_3 is a low-refractive-index and the TiO_2 a high-refractive-index material.²⁰ In mixed oxides²¹ (Al_2O_3 and TiO_2) and $\text{Al}_2\text{O}_3 / \text{TiO}_2$ nanolaminates,²² tailored optical properties varying from Al_2O_3 to TiO_2 with gradual composition change have been demonstrated. Electrical properties^{23,24} can be tuned by adjusting either the TiO_2 fraction^{25,26} or the bilayer thickness^{27,28,29,30} or with an interfacial layers.³¹

The effect of alloying elements on controlling the grain size is well known in bulk materials.³² In ALD, for example, aluminium oxide is known to prevent or retard the growth of crystallites by preventing the nucleation events,^{33,34} thus reducing the surface roughness of the film.^{9,12}

Nanolaminates have been reported to have adjustable mechanical properties, such as hardness and elastic modulus.^{35,36,37,38,39} They have been reported to adhere to substrates better than some reference films.^{40,41} Better corrosion resistance^{41,42,43,44} and thermal stability^{45,46} have also been reported for nanolaminates.

Although ALD Al_2O_3 and TiO_2 have been widely studied both as such and as nanolaminates, little is known on how composition and morphology of the nanolaminate film influence residual stress, adhesion and mechanical properties. The idea of residual stress adjustment has been introduced in $\text{Al}_2\text{O}_3 / \text{TiO}_2$ multilayer materials already in 2005⁴⁷ and since then scattered residual stress data has been published, for example as a function of nanolaminate thickness for films grown at 100 °C,⁴⁸ and for nanolaminates and mixed oxides grown at 220 °C.⁴⁹ Mechanical properties such as elastic modulus and hardness has been studied as a function of bilayer thickness using nanoindentation for films grown at 200 °C³⁹ and elastic modulus by bulge and shaft loading test.⁴⁹ The $\text{Al}_2\text{O}_3 / \text{TiO}_2$ nanolaminate adhesion has been studied by indentation on stainless steel substrate,^{41,40} and for reference ALD Al_2O_3 and ALD TiO_2 materials on silicon⁵⁰ and on polymeric substrate.⁵¹ Since there is no systematic data on residual stress, adhesion and mechanical properties of $\text{Al}_2\text{O}_3 / \text{TiO}_2$ nanolaminates on silicon as a function of ALD temperature, total film thickness, bilayer thickness and TiO_2 fraction, the purpose of this work was to accumulate this knowledge.

Another related publication continues on the same samples; reporting on the thermal conductivity of Al₂O₃ / TiO₂ layers.⁵²

II. EXPERIMENTAL

A. *Sample preparation*

The ALD nanolaminates composed of sequential Al₂O₃ and TiO₂ layers (later called ATO nanolaminates) and reference Al₂O₃ and TiO₂ films, were grown in a top-flow Picosun™ R-150 ALD reactor with three reactant lines. Precursors were trimethylaluminum (Me₃Al), titanium tetrachloride (TiCl₄) and deionized water.

Nitrogen (purity > 99.999%) was used both as a purge gas and for flushing the reactant lines with a constant 200 sccm flow. Electronic grade Me₃Al and TiCl₄ precursors were purchased from SAFC Hitech. The Me₃Al and TiCl₄ precursor bubblers were cooled with a Peltier element to about 17 and 14 °C, respectively. Water was used at room temperature without cooling. Precursor dose and purge times were 0.1 and 4.0 seconds, respectively, for Me₃Al, TiCl₄ and H₂O.

ALD films were grown on 380 ± 5 μm thick double side polished (DSP) and 675 ± 15 μm thick single side polished (SSP) 150 mm, p-type (100) silicon wafers from Okmetic Oyj. Before the film growth, the silicon wafers were cleaned using RCA-cleaning [SC-1 (NH₃:H₂O₂:H₂O), HF-dip (1 %) and SC-2 (HCl:H₂O₂:H₂O) as described in Ref. ⁵³], covering the wafers with a chemical oxide.

For the reference Al₂O₃⁵³ and TiO₂ (some of the results from Ref.⁵⁴) films the growth temperature was varied from 110 to 300 °C while the total thickness was kept constant at about 100 nm. The ‘standard’ ATO nanolaminate with 60 % of TiO₂, was grown at 200 °C, targeting for 5 nm bilayer thickness, composed of 2 nm Al₂O₃ and 3 nm TiO₂

sublayers.⁵⁵ The nanolaminate structure started with growth of an Al₂O₃ layer followed by growth of TiO₂. There was no bottom layer in the nanolaminate, except for the chemical oxide formed during the cleaning sequence. The nanolaminate structure was capped with about 2 nm of Al₂O₃. Al₂O₃ capping was used similarly as in the nanolaminate test series of 2009.⁵⁵ Four different sample sets were designed and fabricated, where one parameter at a time was varied: (1) the growth temperature from 110 to 300 °C, (2) the TiO₂ fraction from 0 to 100 %, (3) the nominal bilayer thickness from 0.1 to 100 nm, and (4) the nanolaminate thickness from 20 to 300 nm. The amount of cycles needed to grow the laminate structure with a desired target thickness was calculated from the growth per cycle (GPC) values of the reference Al₂O₃ and TiO₂ samples grown in 700 and 1400 cycles, respectively, with measured thicknesses of 53.4, 60.6, 67.3, 67.5 and 63.1 nm for Al₂O₃ and 70.4, 58.4, 55.2, 72.5 and 67.2 nm for TiO₂ grown at temperatures 110, 150, 200, 250 and 300 °C, respectively. Linearly increasing thickness was assumed for the ATO nanolaminate when experiments were designed.

B. Characterization

The thickness and refractive index was analysed with spectroscopic reflectometry FilmTek 4000 using wavelength range 400 – 1600 nm. Refractive index was reported for 633 nm wavelength. Thickness and density were analysed with x-ray reflectivity (XRR) and crystallinity was studied by grazing incidence x-ray diffractometry (GIXRD) as described in Ref. ¹⁴. Both the XRR and the GIXRD measurements were performed using a Philips X'Pert Pro diffractometer with parallel beam conditions, and x-ray wavelength, acceleration voltage and anode current Cu-K_α, 40 kV and 40 mA, respectively. Thickness and density values were determined by simulating XRR curves

with the software X'Pert Reflectivity.

The film composition and impurities were analysed with time-of flight elastic recoil detection analysis (TOF-ERDA)⁵⁶ and Rutherford backscattering spectrometry (RBS) using 2 MeV He beam.

Residual stress of the ALD films on silicon was determined with surface profilometry Veeco Dektak V200-Si and wafer curvature method using Stoney's equation as described in Ref. ⁵³ The wafers were scanned parallel and perpendicular to the wafer flat using a 120 mm scan length. The wafer curvature was also measured with TOHO FLX-2320 to acquire thermal properties by in-situ heating the as-grown wafers. The measurement started max. 30 minutes after taking the wafer from the ALD tool and were conducted under continuous nitrogen flow from room temperature up to 500 °C. The measurement was repeated three times consecutively. The scan length was 120 mm and the measurement direction was parallel to the wafer flat. The residual stress values are given with the maximum measurement uncertainty, as calculated in Ref. ⁵³, taking into account the uncertainty in the film and the substrate thicknesses in addition to the wafer curvature measurement.

Scratch testing was carried out to evaluate the adhesion performance of the ALD film using a CSM Micro-Combi tester. A Rockwell C diamond tip with a radius of 20 µm was used in scratch testing with increasing scratch force from 0.05 to 1.3 N and loading rate of 4.17 N/min. The scratch length was 3.0 mm and three scratches per sample were carried out. Four critical loads for adhesion were determined as described in Ref. ⁵⁰, namely L_{CSi1} , L_{CSi2} , L_{CALD1} , L_{CALD2} representing the critical loads for the silicon substrate failure and the film delamination.

The mechanical behaviour of the ATO nanolaminates was studied by nanoindentation using a TriboIndenter® TI-900 (Hysitron, Inc.) nano-mechanical testing system, fine-tuned to eliminate the mechanical, acoustic and electric noise as described in detail in Ref. ⁵⁷ for ALD Al₂O₃ films. The instrument was inside a semi-clean room under constant laminar airflow to minimise the possible thermal drift during the measurement. Five indents were performed under displacement-control at three preselected depths (40, 60, and 80 nm). The segment time at loading, peak-depth holding and unloading was set as 10, 5 and 5 seconds, respectively. Here, the contact modulus, which reflects the elastic response of the whole system including the sample, the indenter, as well as the load frame, is reported. The instrument stability and indentation repeatability were monitored by repeatedly performing a series of 25 indents into a piece of Si wafer during the measurement period.

III. RESULTS

A. Thin film characterization

1. Al₂O₃, TiO₂ and ATO temperature series

The thickness, refractive index, density, crystalline structure and chemical composition of ATO nanolaminates and reference ALD Al₂O₃ and TiO₂ films were characterized at a temperature range from 110 to 300 °C (Al₂O₃ from Ref. ⁵³ and some of the TiO₂ and ATO characterization results from Ref. ⁵⁴ and ¹⁴, respectively). The results are presented in Table 1. The target thickness for total ATO nanolaminate, reference Al₂O₃ and TiO₂ films was 100 nm, while the target thicknesses for the Al₂O₃ and TiO₂ sublayers were 2 and 3 nm, respectively, targeting for 60 % TiO₂ fraction and 5 nm bilayer thickness, throughout the temperature range. The GPC values were calculated by dividing the sublayer thicknesses measured by XRR with the number of growth cycles.

TABLE 1. Thin film characterization results as a function of the growth temperature for ALD Al₂O₃, TiO₂ and ATO nanolaminate. The pulse sequence for the growth was (0.1-4.0) s for pulse and purge of TMA, TiCl₄ and H₂O. The GPC values, for Al₂O₃ and TiO₂, were calculated from thicknesses measured by reflectometer divided by the number of growth cycles. For the nanolaminate the GPC values were calculated from sublayer thicknesses measured by XRR divided by the number of growth cycles in the sublayer. Some of the Al₂O₃, ATO and TiO₂ characterization results were published already in References ^{53,54}.

ALD film	Growth temperature [°C]	Growth cycles				Al ₂ O ₃ cap	Growth per cycle [nm]		Refractive index	XRR density [g/cm ³]	TOF-ERDA Chemical composition [atm.%]						GIXRD	Source	
		NL super cycles	Al ₂ O ₃		TiO ₂		Al ₂ O ₃	TiO ₂			H	C	Cl	O	Al	Ti			
			Al ₂ O ₃	TiO ₂	Al ₂ O ₃														TiO ₂
Al ₂ O ₃	110	-	1283	-	-	0.0732	-	1.615	2.85	11.3	0.94	-	53.9	33.9	-	-	53		
	150	-	1137	-	-	0.0841	-	1.638	2.95	5.6	0.50	-	58.1	35.8	-	-	53		
	200	-	1037	-	-	0.0928	-	1.649	3.05	2.5	0.24	-	58.2	39.0	-	-	53		
	250	-	1037	-	-	0.0936	-	1.655	3.10	1.4	0.15	-	60.0	38.4	-	-	53		
	300	-	1109	-	-	0.0897	-	1.657	3.10	1.0	0.18	-	59.6	39.2	-	-	53		
ATO	110	20	26	58	26	0.0785	0.0500	2.106	3.36	4.7	0.25	1.00	61	13	20	-	this work		
	150	20	23	69	23	0.0913	0.0429	2.160	3.40	2.2	0.15	0.70	62	14	22	-	this work		
	200	20	21	74	21	0.0881	0.0405	2.181	3.53	1.0	0.12	0.30	63	14	22	-	this work		
	250	20	21	59	21	0.0905	0.0373	2.125	3.54	0.5	0.14	0.07	62	18	19	-	this work		
	300	20	22	64	22	0.0909	0.0328	2.135	3.46	0.3	0.07	0.03	62	18	19	-	this work		
TiO ₂	110	-	-	1924	-	-	0.0509	2.417	3.70	1.0	0.20	1.90	65	-	32	-	54		
	150	-	-	2313	-	-	0.0429	2.452	3.75	0.3	<0.10	0.80	65	-	34	-	this work		
	200	-	-	2467	-	-	0.0408	2.603	3.80	0.2	<0.10	0.34	66	-	34	anatase	54		
	250	-	-	1953	-	-	0.0522	2.585	3.75	0.2	0.19	<0.05	66	-	33	anatase	this work		
	300	-	-	2124	-	-	0.0497	2.731	3.85	<0.05	<0.05	<0.05	67	-	33	anatase	54		

The GPC for Al₂O₃ sublayer followed approximately the same trend as a function of ALD temperature as reference ALD Al₂O₃⁵³ where the GPC increased with increasing ALD temperature until 250 °C after it decreased. For the TiO₂ sublayer, the GPC decreased with increasing ALD temperature. The same GPC trend was observed for the reference ALD TiO₂ at temperature range from 110 to 200 °C. After this an abrupt rise in GPC was detected, the GPC being approximately at 0.02 nm higher for reference TiO₂ than ATO TiO₂ sublayer at 250 and 300 °C. The total ATO nanolaminate thickness (Table 2) was approximately constant at temperature range from 110 to 200 °C, after which thinner films were measured, and measured thickness deviated from targeted 100 nm thickness for films grown at 250 and 300 °C. The reflectometry measurements and total thicknesses calculated from XRR sublayer thicknesses were in line. The film non-uniformity (1σ) was about 2.0 % for films grown at 110 to 200 °C and improved to 1.1 % for film grown at 300 °C.

TABLE 2. Thin film characterization results for ATO nanolaminates as a function of the (1) ALD temperature, (2) TiO₂ fraction, (3) bilayer thickness and (4) total nanolaminate thickness. Some of the characterization results from series (3) bilayer thickness were published already in Ref. ¹⁴. Some ATO temperature series results, presented already in TABLE 1, are repeated here for completeness.

Varied parameter	Growth temperature [°C]	Growth cycles				Reflectometry, 5 pts					XRR thickness [nm]		XRR density [g/cm ³]		XRR roughness [nm]		Growth per cycle (nm)		GIXRD observed peaks
		NL cyc	Al ₂ O ₃		Al ₂ O ₃ cap	Thickness [nm]	St.dev [nm]	St.dev. [%]	Refractive index	St.dev.	Al ₂ O ₃	TiO ₂	Al ₂ O ₃	TiO ₂	Al ₂ O ₃	TiO ₂	Al ₂ O ₃ ¹	TiO ₂ ¹	
			cyc	TiO ₂ cyc															
(1) ALD temperature	110	20	26	58	26	99.5	2.0	2.0	2.106	0.008	2.04	2.90	2.80	3.60	0.5	0.5	0.0785	0.0500	-
	150	20	23	69	23	100.3	2.0	2.0	2.160	0.008	2.20	2.86	2.90	3.80	0.1	0.1	0.0913	0.0429	-
	200	20	21	74	21	93.4	1.9	2.0	2.181	0.007	2.15	2.74	2.95	3.80	0.3	0.6	0.0881	0.0405	-
	250	20	21	59	21	77.0	1.1	1.4	2.125	0.004	1.70	2.40	3.00	3.85	0.1	0.1	0.0905	0.0373	-
	300	20	22	64	22	72.9	0.8	1.1	2.135	0.003	1.7	2.40	3.10	3.85	0.1	0.1	0.0909	0.0328	-
(2) TiO ₂ fraction	200	0	1040	0	21	97.9	1.8	1.8	1.643	0.002	98.00	-	3.00	-	0.6	-	0.0942	-	-
	200	20	41	25	21	92.8	1.8	1.9	1.853	0.003	3.89	0.85	2.95	3.90	0.3	0.5	0.0910	0.0400	-
	200	20	31	49	21	92.5	1.9	2.1	2.015	0.005	2.95	1.88	2.90	3.80	0.3	0.7	0.0903	0.0402	-
	200	20	21	74	21	93.4	1.9	2.0	2.181	0.007	2.15	2.74	2.95	3.80	0.3	0.6	0.0881	0.0405	-
	200	20	10	99	21	92.6	2.2	2.4	2.346	0.008	0.95	3.90	2.95	3.80	0.1	0.5	0.0850	0.0404	-
	200	0	0	2467	21	100.0	2.5	2.5	2.522	0.016	-	98.50	-	3.70	-	1.4	-	0.0399	(101)
(3) Bilayer thickness	200 ²	1000	1	1	21	128.9	2.5	1.9	1.965	0.004	138.5	-	3.35	-	0.9	-	0.0685	-	-
	200 ²	400	1	3	21	83.1	1.4	1.7	2.231	0.003	94.0	-	3.70	-	0.9	-	0.0580	-	-
	200 ²	200	3	6	21	99.9	1.4	1.4	2.118	0.004	110.5	-	3.60	-	0.8	-	0.0607	-	-
	200	133	4	9	21	89.5	1.8	1.9	-	-	0.38	0.38	3.05	3.90	0.3	0.3	0.0950	0.0422	-
	200	100	5	12	21	90.6	1.4	1.5	2.134	0.004	0.49	0.48	3.10	4.00	0.4	0.3	0.0980	0.0400	-
	200	50	10	25	21	90.5	1.4	1.5	2.129	0.004	1.00	0.93	2.90	3.90	0.2	0.8	0.1000	0.0372	-
	200	20	26	62	21	93.9	1.6	1.7	2.097	0.006	2.40	2.45	3.10	3.90	0.7	0.6	0.0885	0.0411	-
	200	10	52	123	21	96.4	1.7	1.8	2.091	0.006	5.25	4.50	2.95	3.75	0.3	0.8	0.0904	0.0407	-
	200	5	104	247	21	98.9	1.6	1.6	2.092	0.007	9.75	9.65	2.95	3.75	0.5	0.8	0.0913	0.0401	-
	200	2	259	617	21	104.2	1.7	1.6	2.110	0.008	23.70	24.50	2.95	3.80	0.5	0.8	0.0915	0.0397	-
	200	1	519	1233	21	-	-	-	-	-	50.00	48.30	2.95	3.75	0.5	0.8	-	-	(101), (004), (200), (105)
(4) Total thickness	200 ³	4	21	74	21	-	-	-	-	-	1.90	3.10	3.80	3.80	0.3	0.3	0.0905	0.0419	-
	200	10	21	74	21	48.9	1.2	2.5	2.154	0.010	2.10	2.90	3.00	3.70	0.3	0.3	0.1000	0.0392	-
	200	20	21	74	21	93.4	1.9	2.0	2.181	0.007	2.15	2.74	2.95	3.80	0.3	0.6	0.0881	0.0405	-
	200	60	21	74	21	278.4	5.0	1.8	2.197	0.008	1.90	2.95	3.10	3.80	0.3	0.3	0.0905	0.0399	-

¹ GPC calculated from the XRR sublayer thickness divided by the number of growth cycles

² Mixed oxide

The refractive index of the nanolaminate was expected to slightly increase with increasing ALD temperature on the basis of the results from the reference Al_2O_3 and TiO_2 , presented in Table 1. According to the reflectometry measurements refractive index reached a maximum value at 200 °C and thereafter decreased. The main reason was that the nanolaminate contained less TiO_2 at higher temperatures than expected, resulting in a lower refractive index.

The Al_2O_3 and TiO_2 sublayer densities presented in Table 2, were in line with the density values measured for the reference Al_2O_3 ⁵³ and TiO_2 ⁵⁴ samples. The total nanolaminate density had a local maximum around 250 °C, presented in Table 1.

An approximately constant TiO_2 fraction, around 60 % was measured for nanolaminates grown at ALD temperatures from 110 to 200 °C. TiO_2 fraction dropped to around 50 % at higher temperatures, which differs from the targeted 60 %. Titanium and TiO_2 concentrations calculated from TOF-ERDA and XRR results were in line as presented in Figure 2a. The impurity concentrations decreased with increasing growth temperature as presented in Table 1. The hydrogen content was 4.7 at-% at 110 °C and decreased to 0.3 at-% at 300 °C. Carbon levels were less than 0.3-at% at 110 °C and decreased further with increasing ALD temperature. The chlorine levels, measured with RBS decreased from 1 at-% for film grown at 110 °C to 0.03 at-% at 300 °C. The impurity levels of the nanolaminates were somewhat lower than expected on basis of the rule of mixture, as presented in Figure 3a.

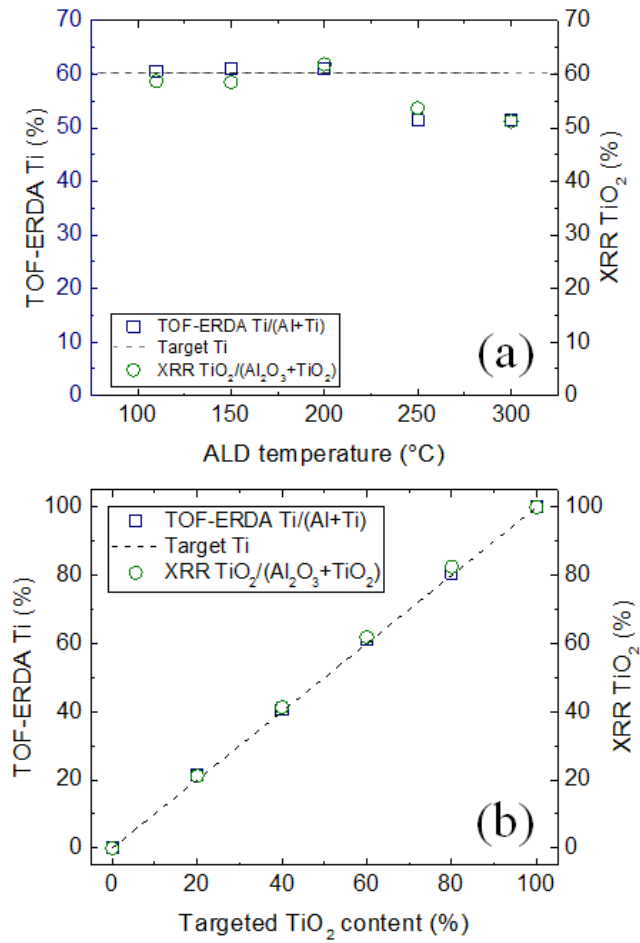
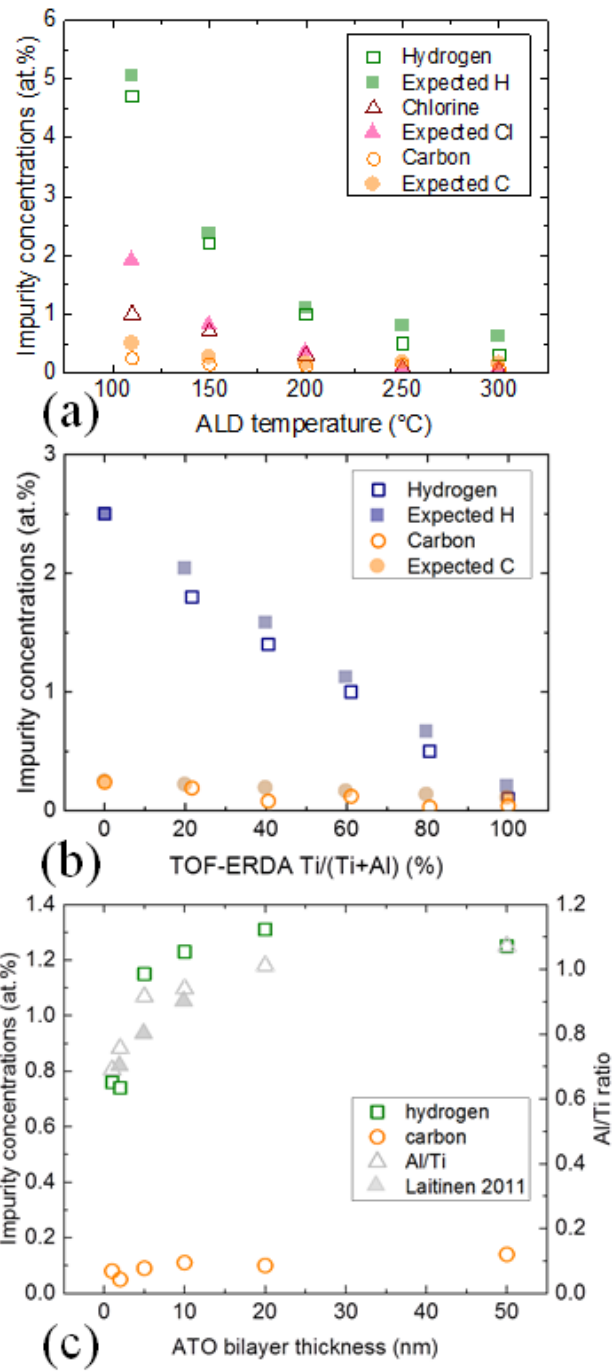


FIG. 2. (Color online) Ti and TiO₂ concentrations measured with TOF-ERDA and XRR, respectively as a function of the (a) ALD temperature and (b) TiO₂ fraction.

As no crystalline peaks were observed with GIXRD, the nanolaminates were concluded to be amorphous through the ALD temperature range (Table 1). The reference ALD Al₂O₃ was amorphous⁵³ while the reference TiO₂⁵⁴ had amorphous structure for films grown at 110 to 150 °C and at higher ALD temperatures polycrystalline structure with anatase phase.



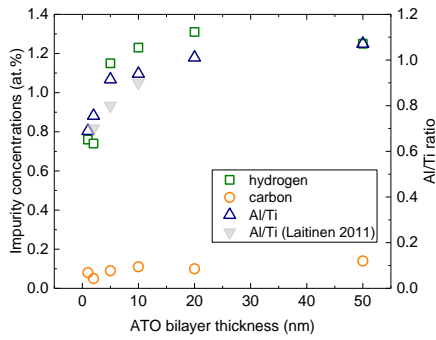


FIG. 3. (Color online) The impurity concentrations measured with TOF-ERDA and RBS (CI) for ATO nanolaminates presented as a function of (a) ALD temperature, while keeping the total thickness, bilayer thickness and TiO_2 fraction constant, and (b) TiO_2 fraction, while ALD temperature, total nanolaminate and bilayer thickness were kept constant, and (c) ALD bilayer thickness. The expected impurity concentrations were calculated from impurity values of the reference ALD Al_2O_3 and TiO_2 films using the rule of mixture.

2. ATO TiO_2 fraction series

TiO_2 fraction was varied from 0 to 100 %, while the growth temperature, the bilayer and the total thicknesses were kept constant at 200 °C, 5 nm and 100 nm, respectively. The measurement results are presented in TABLE 2.

GPC values were approximately constant for the TiO_2 sublayer with increasing TiO_2 fraction and were close to the GPC of the reference TiO_2 film grown at 200 °C. For the Al_2O_3 sublayer, the GPC decreased with increasing TiO_2 fraction. The refractive index increased linearly with increasing TiO_2 fraction and it had linear correlation with density values (calculated from the XRR results), as expected. According to XRR, the nanolaminate sublayers were smoother than reference Al_2O_3 and TiO_2 samples, with

roughness of about 0.3 and 0.6 nm for Al₂O₃ and TiO₂ sublayers, respectively. The reference TiO₂ had XRR roughness of 1.4 nm (polycrystalline), while the reference Al₂O₃ had 0.6 nm roughness.

The Ti and TiO₂ fraction, calculated both from TOF-ERDA and XRR measurements, respectively were in accordance with target TiO₂ values as presented in Figure 2b. The hydrogen content decreased from 2.5 to 0.1 at-% with increasing TiO₂ content, as shown in Figure 3b. Similar behaviour was observed with carbon which decreased from 0.24 to 0.04 at-%. The hydrogen level was lower than detected for the reference Al₂O₃. The Cl content was not analysed for the TiO₂ fraction series.

3. *ATO nanolaminate bilayer thickness series*

The nominal bilayer thickness in the nanolaminate was increased from about 0.1 to 100 nm while the total target thickness and the ALD temperature were kept constant at 100 nm and 200 °C, respectively. The target TiO₂ fraction was 50 vol%. The characterisation results are presented in TABLE 2. Discrete sublayers were detected in the nanolaminate with bilayer thickness down to 0.8 nm as analysed earlier¹⁴, while structures with nominal bilayer thickness less than 0.8 nm were in practice mixed oxides. The sample with bilayer thickness of 100 nm was the only sample where polycrystalline structure with anatase phase was detected by GIXRD, the other samples were amorphous.

The TiO₂ fraction was approximately constant measured both with XRR¹⁴ and TOF-ERDA with increasing bilayer thickness. For samples with bilayer thicknesses less than 1 nm, the targeted TiO₂ fraction of 50 vol% was not achieved, because the amount of material grown by a single cycle could not be continuously tuned. Nanolaminates with

thinnest bilayers had lowest impurity content (Figure 3c). The hydrogen content correlated with the Al content in the film.

4. ATO nanolaminate thickness series

The total nanolaminate thickness was varied from 20 to 300 nm while the bilayer thickness, the TiO₂ fraction and the ALD temperature were kept constant at 5 nm, 60 % and 200 °C. The results are presented in TABLE 2. The nanolaminate thickness increased linearly with the number of nanolaminate supercycles. The refractive index and the density of Al₂O₃ and TiO₂ sublayers were approximately constant. All samples were amorphous.

B. Residual stress

The residual stress of ATO nanolaminate decreased from about 470 to 360 MPa with increasing ALD temperature as presented in Figure 4A and Table 3. For comparison, the stress results are also presented for the reference Al₂O₃ from Ref. ⁵³ and the TiO₂ samples as a function of the ALD temperature. In the reference TiO₂, the stress was constant up to 150 °C, after which an abrupt rise was measured and a stress maximum was achieved for samples grown at 200 °C. At higher temperature, the stress of TiO₂, decreased again. The TiO₂ results were in line with corresponding sample series reported in Ref. ⁵⁴. The increase in stress of TiO₂ coincides with transition to crystalline anatase.

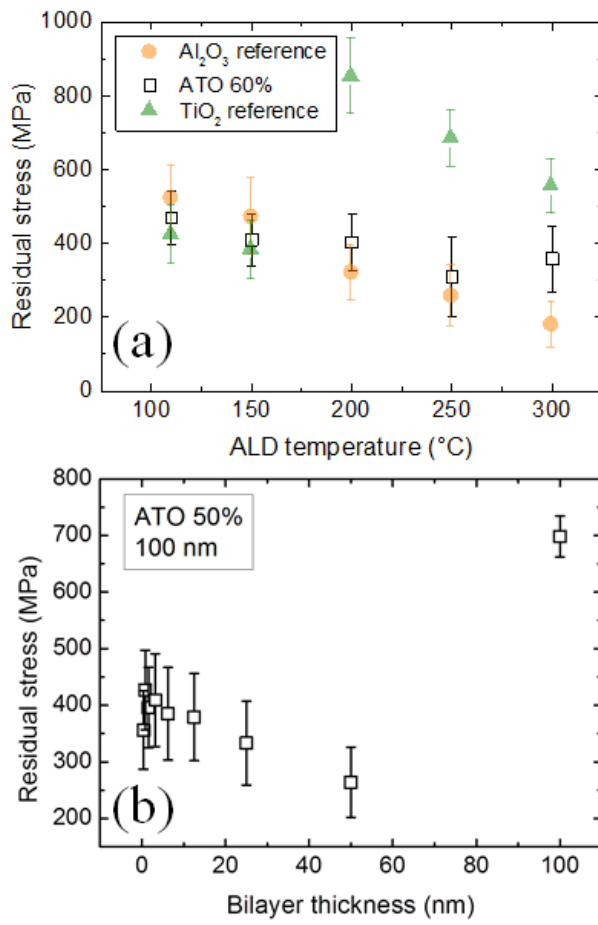


FIG. 4. (Color online) The residual stress of the ATO nanolaminate as a function of the (a) ALD temperature, and (b) bilayer thickness. Error bars present maximum measurement uncertainty as explained in the II. Experimental section.

TABLE 3. Residual stress, contact modulus, hardness and critical load values presented as a function of ALD temperature, TiO₂ fraction, bilayer thickness and total nanolaminate thickness. Same values are presented also for reference ALD Al₂O₃, ALD TiO₂ and TAO nanolaminate grown at 200 °C. Residual stress results present average stress with maximum measurement uncertainty. Contact modulus and hardness values present average of fifteen measurements with standard deviation. And critical load values present average of three measurements with standard deviation. Some of the Al₂O₃ and TiO₂ results were from Ref. ⁵⁰.

	ALD temperature [°C]	TiO ₂ fraction [%]	Total XRR thickness [nm]	Bilayer thickness [nm]	Residual stress [MPa]	Contact Modulus [GPa]	Hardness [GPa]	LCSi1 [mN]	LCSi2 [mN]	LCALD1 [mN]	LCALD2 [mN]
Silicon reference	-	-	-	-	-	147	9.4	580 ± 20	610 ± 15	-	-
(1) ALD temperature	110*	60	98.9	5.0	470 ± 80	146 ± 6	6.9 ± 0.0	-	859 ± 7	1018 ± 60	1140 ± 110
	150*	60	101.2	5.0	410 ± 70	145 ± 3	7.5 ± 0.1	-	845 ± 7	1065 ± 40	1202 ± 35
	200*	60	97.8	5.0	400 ± 80	146 ± 9	7.5 ± 0.0	-	810 ± 3	1013 ± 15	1089 ± 80
	250*	60	82.0	5.0	310 ± 110	156 ± 5	8.4 ± 0.1	-	756 ± 5	1018 ± 10	1187 ± 55
	300*	60	82.0	5.0	360 ± 90	152 ± 3	8.7 ± 0.1	-	773 ± 6	1002 ± 50	1170 ± 10
(2) TiO ₂ fraction	200	20	92.8	5.0	320 ± 220	151 ± 7	8.4 ± 0.3	-	-	-	-
	200	40	92.5	5.0	340 ± 220	153 ± 3	8.0 ± 0.2	-	-	-	-
	200	60	93.4	5.0	320 ± 220	146 ± 9	7.5 ± 0.0	-	-	-	-
	200	80	93.6	5.0	340 ± 220	148 ± 3	7.1 ± 0.1	-	-	-	-
(3) Bilayer thickness	200	50	138.5	mixed	400 ± 170	147 ± 1	8.0 ± 0.2	-	-	-	-
	200	50	94.0	mixed	390 ± 240	153 ± 3	7.8 ± 0.1	-	-	-	-
	200*	50	92.0**	mixed	360 ± 70	-	-	-	-	-	-
	200	50	110.5	mixed	420 ± 210	153 ± 2	7.8 ± 0.1	-	-	-	-
	200*	50	89.9**	0.8	430 ± 70	-	-	-	-	-	-
	200	50	97.0	1.0	410 ± 230	152 ± 4	7.9 ± 0.0	-	-	-	-
	200*	50	87.9**	1.6	400 ± 70	-	-	-	-	-	-
	200	50	96.5	2.0	400 ± 220	145 ± 4	8.0 ± 0.1	-	-	-	-
	200*	50	90.1**	3.2	410 ± 80	-	-	-	-	-	-
	200	50	97.0	5.0	330 ± 220	151 ± 1	8.0 ± 0.0	-	-	-	-
	200*	50	89.5**	6.3	390 ± 80	-	-	-	-	-	-
	200	50	97.5	10.0	320 ± 210	155 ± 1	8.2 ± 0.2	-	-	-	-
	200*	50	95.4**	12.5	380 ± 80	-	-	-	-	-	-
	200	50	97.0	20.0	290 ± 200	151 ± 8	8.2 ± 0.2	-	-	-	-
	200*	50	94.6**	25.0	330 ± 70	-	-	-	-	-	-
200*	50	99.9**	50.0	260 ± 60	-	-	-	-	-	-	
200*	50	96.4	50.0	270 ± 70	156 ± 6	7.9 ± 0.1	-	-	-	-	
200*	50	98.3	100.0	700 ± 40	-	-	-	-	-	-	
(4) Total thickness	200*	60	20.0	5.0	530 ± 310	-	-	460 ± 90	668 ± 14	938 ± 54	1023 ± 20
	200*	60	50.0	5.0	420 ± 130	-	-	-	687 ± 25	1027 ± 75	1135 ± 50
	200*	60	117.8	5.0	380 ± 80	156 ± 9	7.5 ± 0.1	-	810 ± 3	1013 ± 15	1089 ± 80
	200*	60	291.0	5.0	320 ± 40	153 ± 7	7.9 ± 0.2	540 ± 140	1135 ± 7	1148 ± 7	1173 ± 10
Al ₂ O ₃ reference	200	0	98.7	-	400 ± 210	156 ± 6	9.9 ± 0.3	-	817 ± 4	876 ± 60	1015 ± 20
TiO ₂ reference	200	100	99.9	-	780 ± 230	151 ± 4	8.3 ± 0.9	626 ± 91	753 ± 17	987 ± 22	1001 ± 15
TAO	200*	60	91.1	5.0	350 ± 80	-	-	-	829 ± 5	918 ± 5	1110 ± 50

*for residual stress measurements 380 ± 5 μm thick wafer was used

**Film thickness measured with reflectometry

An approximately constant residual stress was measured as a function of TiO₂ fraction for samples grown at 200 °C, as presented in Table 3. The reference sample with 100 % TiO₂ had substantially higher stress value compared to nanolaminates, due to the crystalline nature of the film.

Increasing the bilayer thickness from 0.8 to 50 nm, the residual stress decreased from 430 to 260 MPa, as shown in Figure 4B. An elevated stress of 700 ± 40 MPa was measured for the sample with bilayer thickness of 100 nm, in line with change in film morphology (polycrystalline structure). The stress of mixed oxide samples (bilayer thickness <0.8 nm) was close to the stress value measured for the reference ALD Al₂O₃.

The residual stress values as a function of film thickness, from 50 to 300 nm, were within measurement accuracy of this work, and thus no conclusions can be made on basis of the results, as presented in Table 3.

Upon thermal cycling from room temperature up to 500 °C, of about 100 nm thick, 60% ATO nanolaminate grown at 300 °C, minor stress relaxation was measured. When annealing temperature reached the growth temperature, some amount of tensile residual stress (about 100 MPa) was measured, indicating that besides thermal stress there is growth related stress in the film. At annealing temperatures above 400 °C compressive stress was measured in the stress-temperature curve as presented in Figure 5; this was because of the thermal mismatch between the silicon substrate and the ALD film. As the stress-temperature curve was reversible with little hysteresis and only minor stress relaxation was measured for room temperature values, we conclude that no phase changes occurred during the thermal cycling and the morphological properties of the film were stable up to 500 °C.

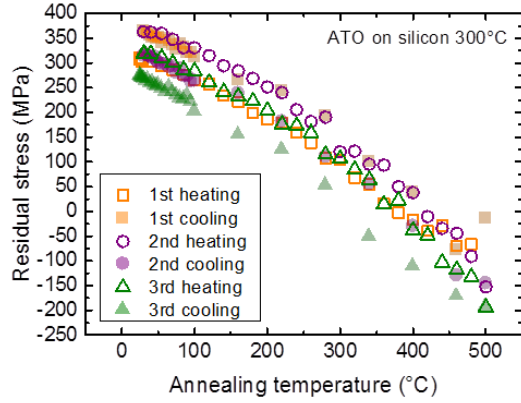


FIG. 5. (Color online) The residual stress as a function of thermal cycling temperature from room temperature up to 500 °C.

C. Adhesion

Critical loads for the delamination of the ATO nanolaminates were measured as a function of the ALD temperature and the total nanolaminate thickness. The results were compared to the values of reference silicon substrate, ALD Al₂O₃^{53,50} and ALD TiO₂⁵⁰ films, and nanolaminate starting with a TiO₂ layer (TAO). The numerical results are presented in Table 3.

For the reference silicon without coating, the first initial failure (L_{CSi1}) and continuous breakage (L_{CSi2}) occurred at critical loads slightly before and close to 600 mN, respectively. The presence of ALD films increased the critical load value L_{CSi2} .

For all ATO films as well as reference ALD films, delamination of the film occurred after breakage of the silicon substrate ($L_{CALD1} > L_{CSi2}$). This indicates a strong adhesion between the nanolaminate and the silicon in all cases. Overall, critical load values (L_{CALD1} and L_{CALD2}) representing the adhesion performance of the ATO films, were at a similar high level as of reference ALD Al₂O₃ and TiO₂ (grown at 200 °C). The only exception was the ATO film with a total thickness of 20 nm, which had the overall lower critical load values compared to other films. The growth temperatures up to 200 °C provided similar critical load values L_{CSi2} ,

but the ATO nanolaminates grown at temperatures from 250 to 300 °C showed slightly lower critical load values.

No significant difference was found between the critical load values nor the delamination behaviour of TAO when compared to ATO laminate (both grown at 200 °C, TiO₂ fraction 60%, and total thickness 100 nm).

D. Contact modulus and hardness

The nanoindentation hardness and contact modulus values are presented in Table 3. The values represent an average of fifteen indents performed under displacement control (indent depth 40 to 80 nm). Since the Poisson's ratio of the laminate was not precisely known, contact modulus instead of elastic modulus is given. Contact modulus represents the combined elastic response of the specimen, indenter and the load-frame of the instrument, and is related to the elastic modulus of the specimen through the Poisson's ratio of both the specimen and the indenter, as well as the elastic modulus of the indenter.

Elastic behaviour of the laminate remained approximately constant, independent of the TiO₂ fraction, bilayer thickness or ALD temperature. Highest hardness values were measured for the lowest TiO₂ fraction and at highest ALD temperature, at 300 °C, while the hardness remained nearly constant with increasing bilayer thickness.

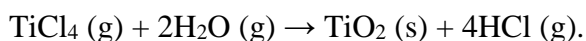
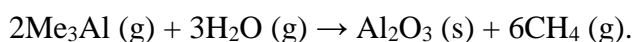
IV. DISCUSSION

A. Short literature review

This work concerns ATO nanolaminates consisting of sublayers grown with the Me₃Al/H₂O and TiCl₄/H₂O processes. The Me₃Al/H₂O was first reported in the late 1980s.⁵⁸ The Me₃Al/H₂O process to grow Al₂O₃ is, because of its near-ideal nature, sometimes considered a “model” for ALD,^{3,6,59,60} and it might be the most widely used ALD process.⁶¹ A dedicated review article has been written on its reaction mechanisms⁶² and the reaction mechanisms is further discussed in our recent publications.^{53,63}

The TiCl₄/H₂O has been known over 45 years, and it may even be the oldest ALD process known^{64,65} and the second-most widely used ALD process.⁶¹ A dedicated review has been written about the reaction mechanisms and “agglomeration phenomenon” in this process, taking place beyond 300 °C.⁶⁶

Taking into account the widespread use of these two processes, there is surprisingly little information available on combining these two processes as ATO. ATO has been used industrially since the 1980s in electroluminescent displays⁶⁷; however for that, chloride reactant is used also for the Al₂O₃ component. The first report of ATO films by combining the Me₃Al and TiCl₄-based processes is from year 1999⁴² and several studies have been made thereafter.^{20,68,69,70} At VTT, the ATO process was taken in use in mid 2000s. Overall reaction equations are:



Interesting findings have been made regarding combining the Me₃Al/H₂O and TiCl₄/H₂O ALD processes as ATO nanolaminates or mixed oxides. From TOF-ERDA results, Laitinen et al.⁷¹ has reported, a smaller Al/Ti ratio with decreasing bilayer thickness (down to 2 nm). The change in Al/Ti-ratio was proposed to be either due to enhanced GPC (called growth rate in Ref. ⁷¹) of TiO₂, reduced GPC of Al₂O₃ during the first cycles, or etching of Al₂O₃ by TiCl₄. Sintonen et al. ¹⁴, on the basis of extended XRR measurements for the same sample series as in this work, reported that down to a bilayer thickness of about 0.8 nm (nominal thickness of 0.4 nm for both constituent oxides), the structure remains a laminate that consists of two distinctive and separate layers. Both amorphous and crystalline ALD TiO₂ sublayers have been reported for ATO nanolaminates depending on TiO₂ thickness, ALD temperature and substrate.^{39,69,72,73}

B. ALD growth

The GPC of the TiO₂ sublayer in the ATO films had a different trend with temperature than the GPC in thicker pure TiO₂ films, as shown in Table 1. It has been observed that the GPC in the TiCl₄/H₂O process decreases with temperature, then increases and goes through a maximum, after which it decreases again.⁷⁴ The increase in GPC occurs at the same time with crystallization.⁷⁵ For the TiO₂ sublayer in the ATO films, no intermediate increase was observed; instead, there was a continuously decreasing trend. The thin TiO₂ sublayer films in ATO remained amorphous up to 300 °C (Table 1), so the difference in GPC of TiO₂ in ATO and TiO₂ as such is most likely related to differences in the film crystallinity. Because of the smaller GPC of TiO₂ in ATO than in thicker TiO₂ films used for reference, the resulting TiO₂ contents in the films deposited at >200 °C were less than expected, roughly 50 vol-% instead of the targeted 60 vol-%.

The ATO films were, throughout the temperature range used in this work (110 to 300 °C), somewhat purer than expected on the basis of the impurities in thicker Al₂O₃ and TiO₂ films (calculated using the rule of mixture). At 110 °C, chlorine content was significantly lower than expected from the impurity content of the reference oxides. Hydrogen content was lower throughout the temperature range used. The source of carbon and chlorine are the Me₃Al and TiCl₄ reactants, respectively. The hydrogen originates mostly from the H₂O precursor.⁶³ The interfaces between Al₂O₃ and TiO₂ seem to have lower impurity contents (Cl, C, H) than the bulk materials.

From the results obtained for the TiO₂ fraction series and ATO bilayer thickness series (both at 200 °C), one can estimate how Al₂O₃ grows on TiO₂. The average GPC of Al₂O₃ and TiO₂ on a TiO₂ starting surface (data in Table 2) is plotted in Figure 6 for the two series for the conditions a laminate is grown. Overall, it is seen that the average GPC of Al₂O₃ is lower in the beginning of the growth and increases towards a steady value of 0.092 - 0.094 nm. The two series in general agree, with the exception of the first three points of the ATO bilayer

series, which give a significantly higher GPC of Al_2O_3 . Generalizing the main result, the GPC of Al_2O_3 is thus smaller on TiO_2 than it is on itself. Such behaviour has been classified as “substrate-inhibited growth of Type 1”.^{76,3} It has been proposed that the GPC of the $\text{Me}_3\text{Al-H}_2\text{O}$ process depends directly (but not with a 1:1 ratio but rather a 1:3 ratio) on the surface OH group density.^{62,3} Our result therefore suggests that the OH group density at 200 °C on TiO_2 should be lower than it is on Al_2O_3 . Comparison to literature indicates supports the suggestion: for (polycrystalline) TiO_2 , a density of 4.5 OH/nm² has been measured at 200 °C^{77,78} and for Al_2O_3 , a significantly higher density of 7.1 OH/nm.^{2,79} Regarding the first three points of the ATO bilayer thickness series where the GPC of Al_2O_3 was higher (4, 5, and 10 cycles of Al_2O_3 on very thin TiO_2 of 0.4-0.9 nm, TABLE 2), the result differs from the series and is more difficult to explain. While the reason for the higher GPC of Al_2O_3 remains unknown at the moment, we speculate that, in that case, the very thin TiO_2 layer may differ in character as compared to thicker, more bulk-like, continuous TiO_2 layers, leading to different reaction mechanisms during the Me_3Al reaction and, as a result, a higher GPC. The unusually high density of TiO_2 measured for the thinnest layers by XRR (see TABLE 2) is in accord with the special nature of the thinnest TiO_2 layers.

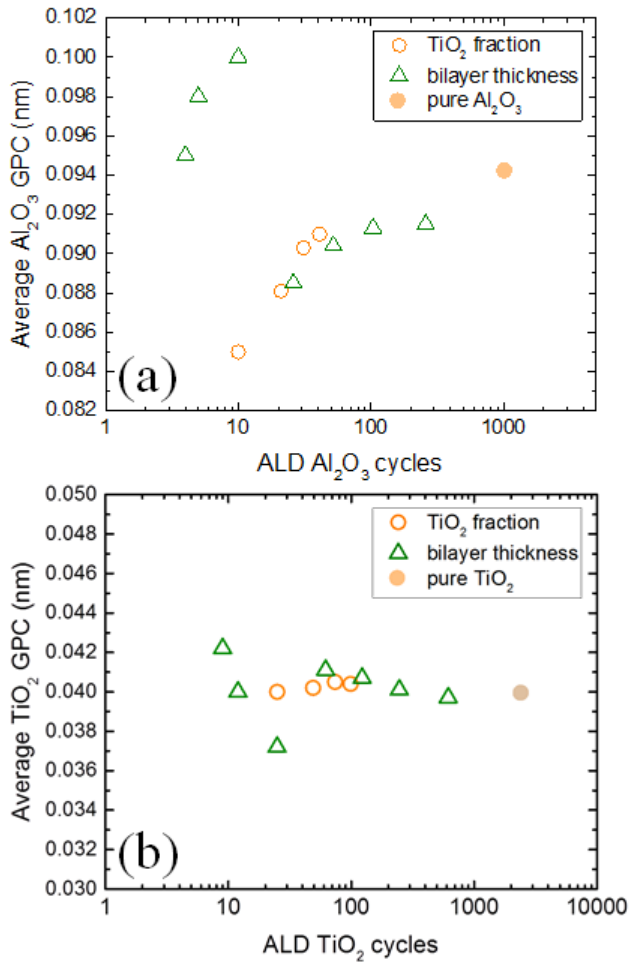


FIG. 6. (Color online) The average GPC for (a) Al₂O₃ and (b) TiO₂ as a function of growth cycles.

Similarly as analysed for Al₂O₃ on TiO₂, the results can also be used vice versa to analyse the growth of TiO₂ on Al₂O₃. On the basis of the results on Table 2 and Figure 6, it seems that the GPC TiO₂ does not depend significantly on the cycles used. Therefore, and TiO₂ ALD on Al₂O₃ follows the “linear growth” classification,^{76,3} at least as long as TiO₂ remains amorphous. In the light of results, since Al₂O₃ has a smaller GPC on TiO₂ than it has on itself and the GPC of TiO₂ on Al₂O₃ was roughly the same as on TiO₂, it seems evident that from the mechanisms suggested by Laitinen et al.⁷¹, it is the “reduced growth rate” of Al₂O₃ that explains the lower Al/(Al+Ti) ratio in the beginning of ATO nanolaminate growth.

C. Residual stress

All ATO nanolaminates investigated in this work were under tensile residual stress. The residual stress of ATO decreased with increasing ALD temperature, from 470 MPa at 110 °C and 360 MPa at 300 °C. The TiO₂ fraction did not influence the residual stress of the nanolaminate (grown at 200 °C) as long as sublayers remained amorphous. Our results are in line with those of Berdova et al.⁴⁹ for films grown at 220 °C (50% of TiO₂, 4 nm bilayer thickness, residual stress ~450 MPa). And agree with the results of Behrendt et al.⁴⁸ for ATO films grown at 100 °C (50% of TiO₂, 2 nm bilayer thickness, residual stress ~400 MPa) where residual stress was reported to be independent of the film thickness.

In laminated structure with constant overall composition (50% TiO₂), the residual stress decreased with increasing bilayer thickness as long as bilayers remained amorphous. Substantially higher stress was measured from the sample with a bilayer thickness of 100 nm due to a transition from amorphous to crystalline TiO₂. The transition occurs at bilayer thickness greater than 50 nm. The tunability of the residual stress can be useful especially when the TiO₂ content and thus the refractive index in the nanolaminate need to be fixed.

For the mixed oxides with nominal bilayer thickness less than 0.8 nm, approximately a constant stress was measured (360 MPa). The maximum residual stress was measured for the sample with 0.8 nm bilayer thickness, in line with the observation that maximum tensile stress occurs when the film becomes completely continuous.⁸⁰ Our results are in line with literature for mixed oxide grown at 220 °C.⁴⁹

It is interesting also to compare our film stress results to earlier ATO nanolaminate film stress results. According to Maula et al.⁴⁷, the stress of TiO₂ and Al₂O₃, grown at 285 °C on an unknown substrate, were 190 MPa (tensile) and -65 MPa (compressive). (In our work, we use the convention that tensile stress is positive and compressive stress is negative in magnitude.) By stepwise incorporating more amorphous Al₂O₃ into the crystalline TiO₂, film stress could be diminished to approximately zero level (on the unknown substrate) at Al₂O₃ / TiO₂ ratio of

about 0.17. In our work, stress of 100 nm films of TiO₂ and Al₂O₃ grown at 200 °C were around 800 and 400 MPa, respectively, on silicon substrates. By incorporation of about 20% of Al₂O₃ in TiO₂, stress decreased significantly (by ~400 MPa), down to the level typical of the amorphous nanolaminates. It is likely that an accurate control of the Al₂O₃ fraction/sublayer thickness in more TiO₂-rich films would allow an accurate tuning of film stress in our case, too. Although the absolute stress values differed in our work compared to that of Maula et al.⁴⁷ (due to the use of different substrate materials) and we could not approach zero stress in this work; we conclude that the decreasing trend of tensile stress of TiO₂ with incorporation of Al₂O₃ was identical in the two works.

D. Adhesion

The amorphous ALD nanolaminate films had good adhesion properties on silicon, necessary to achieve the required functionality in MEMS structures. The ATO films were able to withstand similar critical loads before coating failure compared to the reference Al₂O₃ and TiO₂. This performance is in line with earlier study of Kääriäinen et al.⁸¹ on ALD Al₂O₃ and TiO₂ films.

The critical load values, determined in scratch testing for the silicon breakage and coating delamination, showed slightly increasing trend with the increasing coating thickness. However, the ATO film with a total thickness of 20 nm overall had lower critical load values compared to other films. Thinnest film had also the highest tensile residual stress, which might have reduced the critical loads and thus influenced the adhesion performance of the coating.

The growth temperatures up to 200 °C provided equal critical load values. The ATO nanolaminates grown at temperatures from 250 to 300 °C showed slightly lower critical load values. This is related to the previously reported finding that the TiO₂ films grown at 250 °C and higher have lower critical loads in scratch testing than ALD Al₂O₃, behaviour most likely

caused by crystallinity of the films grown in higher temperatures.⁵⁰

No significant difference was found between the critical load values nor the delamination behaviour of TAO when compared to ATO laminate (both grown at 200 °C, TiO₂ fraction 60%, and total thickness 100 nm). Therefore both Al₂O₃ and TiO₂ can be used as the starting layers of ALD growth on RCA-cleaned silicon.

The presence of ALD nanolaminates postponed the breakage of the silicon and increased the critical load value L_{CSi2} . This suggests that the ALD nanolaminates increased the load carrying capacity of silicon, an observation made also for the single layer ALD films in earlier work.⁵⁰

E. Contact modulus and hardness

Contact modulus remained approximately constant; independent of the ALD temperature, TiO₂ fraction, and bilayer thickness. The laminate hardness depended linearly on the total TiO₂ fraction, the softer component in the laminate, as expected.

Varying the bilayer thickness, while keeping the TiO₂ fraction constant, caused no notable changes in the hardness. Our results are approximately similar as in Ref. ³⁹, where no significant changes in elastic modulus were detected with increasing bilayer thickness.

Comparing to the ZnO/Al₂O₃ laminate case by Raghavan et al.³⁷ and Homola et al.³⁸, our case differs. Raghavan et al.³⁷ found that the laminates were the softer the thinner the bilayers, as the ZnO constituent layers in the nanolaminates simultaneously changed from crystalline to amorphous, in line with results of Homola et al.³⁸. In our case, the TiO₂ films were amorphous, and consequently, no changing trend was observed.

In the ATO temperature series, with targeted constant composition of 60% TiO₂, the laminate hardness increased with increasing ALD temperature. This was unexpected, since previously published results for ALD Al₂O₃⁵³ have shown that the increase of hardness with increasing

temperature is marginal after 150 °C. Because of nonlinearity of the ALD ATO growth, the target and measured film composition differed at ALD temperatures above 200 °C, as the measured TiO₂ fraction was 50%. Amorphous TiO₂ is softer than amorphous Al₂O₃; however, crystalline TiO₂ is likely to be harder.⁵⁴ The tendency of TiO₂ grown on Al₂O₃ to crystallize increases, the higher the ALD temperature.⁷³ Although we did not observe crystalline TiO₂ in GIXRD, we consider it likely that the increase in hardness may originate from changes in the structure and nanocrystallinity of TiO₂.

V. CONCLUSIONS

Mixed oxides and nanolaminates were grown from Al₂O₃ and TiO₂ layers by ALD from AlMe₃, TiCl₄ and H₂O reactants. Fewer impurities were detected in ATO nanolaminates compared to the constituent oxide films. The nanolaminates were determined to be under tensile stress. Bilayer thickness and ALD temperature were the major parameters affecting the stress of the ATO layer. The residual stress increased with decreasing bilayer thickness and was independent of the TiO₂ content as long as the laminated structure remained amorphous. With increasing growth temperature the stress decreased. The contact modulus was stable and independent of the growth temperature, TiO₂ fraction and bilayer thickness. Higher growth temperatures provided harder ATO films. Nanolaminates with higher TiO₂ fraction were softer. Nanolaminates were able to withstand equal critical loads in scratch testing compared to the reference ALD Al₂O₃ and TiO₂ on silicon, and the nanolaminates also improved the load carrying capacity of the silicon. The adhesion of the ATO nanolaminates on silicon was good also regarding the functionality required in MEMS devices.

ACKNOWLEDGMENTS

This work has been carried out within the MECHALD project funded by Tekes and is linked to the Finnish Centres of Excellence in Atomic Layer Deposition (ref. 251220) and Nuclear and Accelerator Based Physics (ref. 213503 and 251353) of the Academy of Finland. Parts of these results were presented in oral presentation held at the 19th EuroCVD conference,

September 1-6th 2013, Varna, Bulgaria, and at International Workshop on the Mechanical Behavior of Nanoscale Multilayers, October 1-4th, 2013, Madrid, Spain.

References

- ¹R. L. Puurunen, *Chem. Vapor Depos.*, **20**, 332–344 (2014).
- ²A. A. Malygin, V. E. Drozd, A. A. Malkov, and V. M. Smirnov, *Chem. Vapor Depos.*, **21**, 216–240 (2015).
- ³R. L. Puurunen, *J. Appl. Phys.*, **97**, 121301 (2005).
- ⁴H. B. Profijt, S. E. Potts, M. C. M. van de Sanden, and W. M. M. Kessels, *J. Vac. Sci. Technol. A*, **29**, 50801 (2011).
- ⁵V. Miikkulainen, M. Leskelä, M. Ritala, and R. L. Puurunen, *J. Appl. Phys.*, **113** (2013).
- ⁶S. M. George, *Chem. Rev.*, **110**, 111–131 (2010).
- ⁷J. W. Elam, D. Routkevitch, P. P. Mardilovich, and S. M. George, *Chem. Mater.*, **15**, 3507–3517 (2003).
- ⁸F. Gao, S. Arpiainen, and R. L. Puurunen, *J. Vac. Sci. Technol. A*, **33**, 10601 (2015).
- ⁹M. Ritala, M. Leskelä, L. Niinistö, T. Prohaska, G. Friedbacher, and M. Grasserbauer, *Thin Solid Films*, **249**, 155–162 (1994).
- ¹⁰D. Riihelä, M. Ritala, R. Matero, and M. Leskelä, *Thin Solid Films*, **289**, 250–255 (1996).
- ¹¹M. Ritala, *Appl. Surf. Sci.*, **112**, 223–230 (1997).
- ¹²J. W. Elam, Z. A. Sechrist, and S. M. George, *Thin Solid Films*, **414**, 43–55 (2002).
- ¹³D. R. G. Mitchell, D. J. Attard, K. S. Finnie, G. Triani, C. J. Barbé, C. Depagne, and J. R. Bartlett, *Appl. Surf. Sci.*, **243**, 265–277 (2005).
- ¹⁴S. Sintonen, S. Ali, O. M. E. Ylivaara, R. L. Puurunen, and H. Lipsanen, *J. Vac. Sci. Technol. A*, **32**, 01A111 (2014).
- ¹⁵O. Sneh, R. B. Clark-Phelps, A. R. Londergan, J. Winkler, and T. E. Seidel, *Thin Solid Films*, **402**, 248–261 (2002).
- ¹⁶S. V. Zhukovsky, A. Andryieuski, O. Takayama, E. Shkondin, R. Malureanu, F. Jensen, and A. V. Lavrinenko, *Phys. Rev. Lett.*, **115**, 1–5 (2015).
- ¹⁷J. I. Skarp, “Combination film, in particular for thin film electroluminescent structures,” U.S. Patent No 4,486,487 (4 December 1984).
- ¹⁸T. Suntola and J. Hyvärinen, *Annu. Rev. Mater. Sci.*, **15**, 177–195 (1985).
- ¹⁹A. Rissanen, U. Kantojärvi, M. Blomberg, J. Antila, and S. Eränen, *Sensor Actuat, A-Phys.*, **182**, 130–135 (2012).
- ²⁰S. Zaitso, T. Jitsuno, M. Nakatsuka, T. Yamanaka, and S. Motokoshi, *Appl. Phys. Lett.*, **80**, 2442 (2002).
- ²¹N. Biluš Abaffy, D. G. McCulloch, J. G. Partridge, P. J. Evans, and G. Triani, *J. Appl. Phys.*, **110**, 123514 (2011).
- ²²N. Y. Garces, D. J. Meyer, V. D. Wheeler, Z. Liliental-Weber, D. K. Gaskill, and C. R. Eddy, *J. Vac. Sci. Technol. B*, **32**, 03D101 (2014).
- ²³A. P. Alekhin, A. A. Chouprik, S. A. Gudkova, A. M. Markeev, Y. Y. Lebedinskii, Y. A. Matveyev, and A. V Zenkevich, *J. Vac. Sci. Technol. B*, **29**, 01A302 (2011).
- ²⁴P. F. Siles, M. de Pauli, C. C. Bof Bufon, S. O. Ferreira, J. Bettini, O. G. Schmidt, and A. Malachias, *Nanotechnology*, **24**, 35702 (2013).

- ²⁵I. Jõgi, K. Kukli, M. Kemell, M. Ritala, and M. Leskelä, *J. Appl. Phys.*, **102**, 114114 (2007).
- ²⁶G. Lee, B. K. Lai, C. Phatak, R. S. Katiyar, and O. Auciello, *Appl. Phys. Lett.*, **102** (2013).
- ²⁷Y. S. Kim and S. Jin Yun, *J. Cryst. Growth*, **274**, 585–593 (2005).
- ²⁸P. C. Rowlette and C. A. Wolden, *Thin Solid Films*, **518**, 3337–3341 (2010).
- ²⁹W. Li, O. Auciello, R. N. Premnath, and B. Kabius, *Appl. Phys. Lett.*, **96**, 162907-1–3, (2010).
- ³⁰W. Li, Z. Chen, R. N. Premnath, B. Kabius, and O. Auciello, *J. Appl. Phys.*, **110**, 24106 (2011).
- ³¹G. Lee, B.-K. Lai, C. Phatak, R. S. Katiyar, and O. Auciello, *J. Appl. Phys.*, **114**, 27001 (2013).
- ³²I. Petrov, P. B. Barna, L. Hultman, and J. E. Greene, *J. Vac. Sci. Technol. A*, **21**, S117 (2003).
- ³³D. M. Hausmann and R. G. Gordon, *J. Cryst. Growth*, **249**, 251–261 (2003).
- ³⁴Z. A. Sechrist, F. H. Fabreguette, O. Heintz, T. M. Phung, D. C. Johnson, and S. M. George, *Chem. Mater.*, **17**, 3475–3485 (2005).
- ³⁵A. Madan, Y. Wang, S. A. Barnett, C. Engström, H. Ljungcrantz, L. Hultman, and M. Grimsditch, *J. Appl. Phys.*, **84**, 776 (1998).
- ³⁶M. Ben Daia, P. Aubert, S. Labdi, C. Sant, F. A. Sadi, P. Houdy, and J. L. Bozet, *J. Appl. Phys.*, **87**, 7753 (2000).
- ³⁷R. Raghavan, M. Bechelany, M. Parlinska, D. Frey, W. M. Mook, A. Beyer, J. Michler, and I. Utke, *Appl. Phys. Lett.*, **100**, 191912 (2012).
- ³⁸T. Homola, V. Buršíková, T. V. Ivanova, P. Souček, P. S. Maydannik, D. C. Cameron, and J. M. Lackner, *Surf. Coatings Technol.*, **284**, 198-205 (2015).
- ³⁹I. Iatsunskyi, E. Coy, R. Viter, G. Nowaczyk, M. Jancelewicz, I. Baleviciute, K. Załęski, and S. Jurga, *J. Phys. Chem. C*, **119**, 20591-20599 (2015).
- ⁴⁰E. Marin, A. Lanzutti, M. Lekka, L. Guzman, W. Ensinger, and L. Fedrizzi, *Surf. Coatings Technol.*, **211**, 84–88 (2012).
- ⁴¹E. Marin, L. Guzman, A. Lanzutti, W. Ensinger, and L. Fedrizzi, *Thin Solid Films*, **522**, 283–288 (2012).
- ⁴²R. Matero, M. Ritala, M. Leskelä, T. Salo, J. Aromaa, and O. Forsén, *J. Phys. IV*, **9**, 493–499 (1999).
- ⁴³E. Marin, A. Lanzutti, L. Guzman, and L. Fedrizzi, *J. Coatings Technol. Res.*, **9**, 347–355 (2012).
- ⁴⁴A. I. Abdulagatov, Y. Yan, J. R. Cooper, Y. Zhang, Z. M. Gibbs, A. S. Cavanagh, R. G. Yang, Y. C. Lee, and S. M. George, *ACS Appl. Mater. Interfaces*, **3**, 4593–4601 (2011).
- ⁴⁵P. C. Yashar and W. D. Sproul, *Vacuum*, **55**, 179–190 (1999).
- ⁴⁶H. S. Chang, S. Jeon, H. Hwang, and D. W. Moon, *Appl. Phys. Lett.*, **80**, 3385 (2002).
- ⁴⁷J. Maula, K. Härkönen, and A. Nikolov, “Multilayer material and method of preparing same,” U.S. Patent No. 7,901,736 B2 (8 March 2011).
- ⁴⁸A. Behrendt, J. Meyer, P. van de Weijer, T. Gahlmann, R. Heiderhoff, and T. Riedl, *ACS*

- Appl. Mater. Interfaces*, **8**, 4056-4061 (2016).
- ⁴⁹M. Berdova, T. Ylitalo, I. Kassamakov, J. Heino, P. T. Törmä, L. Kilpi, H. Ronkainen, J. Koskinen, E. Hægström, and S. Franssila, *Acta Mater.*, **66**, 370–377 (2014).
- ⁵⁰L. Kilpi, O. M. E. Ylivaara, A. Vaajoki, J. Malm, S. Sintonen, M. Tuominen, R. L. Puurunen, and H. Ronkainen, *J. Vac. Sci. Technol. A*, **34**, 01A124 (2016).
- ⁵¹T. O. Kääriäinen, P. J. Kelly, D. C. Cameron, B. Beake, H. Li, P. M. Barker, and C. F. Struller, *J. Vac. Sci. Technol. A*, **30**, 01A132 (2012).
- ⁵²S. Ali, T. Juntunen, S. Sintonen, O. M. E. Ylivaara, R. L. Puurunen, H. Lipsanen, I. Tittonen, and S.-P. Hannula, *Nanotechnology*, **27** (2016).
- ⁵³O. M. E. Ylivaara, X. Liu, L. Kilpi, J. Lyytinen, D. Schneider, M. Laitinen, J. Julin, S. Ali, S. Sintonen, M. Berdova, E. Haimi, T. Sajavaara, H. Ronkainen, H. Lipsanen, J. Koskinen, S. P. Hannula, and R. L. Puurunen, *Thin Solid Films*, **552**, 124–135 (2014).
- ⁵⁴J. Lyytinen, X. Liu, O. M. E. Ylivaara, S. Sintonen, A. Iyer, S. Ali, J. Julin, H. Lipsanen, T. Sajavaara, R. L. Puurunen, and J. Koskinen, *Wear*, **342–343**, 270–278 (2015).
- ⁵⁵R. L. Puurunen and H. Kattelus, “ALD ATO nanolaminates with adjustable electrical properties,” in *ALD 2009, 9th International Conference on Atomic Layer Deposition, Monterey, California, USA, July 19-22* (2009).
- ⁵⁶M. Laitinen, M. Rossi, J. Julin, and T. Sajavaara, *Nucl. Instruments Methods Phys. Res. Sect. B Beam Interact. with Mater. Atoms*, **337**, 55–61 (2014).
- ⁵⁷X. Liu, E. Haimi, S.-P. Hannula, O. M. E. Ylivaara, and R. L. Puurunen, *J. Vac. Sci. Technol. A*, **32**, 01A116 (2014).
- ⁵⁸G. S. Higashi and C. G. Fleming, *Appl. Phys. Lett.*, **55**, 1963–1965 (1989).
- ⁵⁹K. Knapas and M. Ritala, *Crit. Rev. Solid State Mater. Sci.*, **38**, 167–202 (2013).
- ⁶⁰T. Weckman and K. Laasonen, *Phys. Chem. Chem. Phys.*, **17**, 17322–17334 (2015).
- ⁶¹V. Miikkulainen, M. Leskelä, M. Ritala, and R. L. Puurunen, *J. Appl. Phys.*, **113**, 21301 (2013).
- ⁶²R. L. Puurunen, *Appl. Surf. Sci.*, **245**, 6–10 (2005).
- ⁶³T. Sajavaara, J. Malm, J. Julin, M. Laitinen, K. Arstila, and R. L. Puurunen, “Origin of hydrogen impurity in Al₂O₃ thin films grown by ALD using Me₃Al and water (D₂O, H₂O) as precursors,” in *AVS Topical Conference on Atomic Layer Deposition*, (2014).
- ⁶⁴S. I. Kol'tsov, *J. Appl. Chem. USSR*, **42**, 5, 975–979 (1969).
- ⁶⁵A. M. Shevyakov, G. N. Kuznetsova, and V. B. Aleskovskii, “Interaction of titanium and germanium tetrachlorides with hydrated silica,” in *Chemistry of high temperature materials. Proceedings of 2nd USSR conference on high temperature chemistry of oxides, November 26-29, 1965, Leningrad, USSR*, pp. 162–168 (1967).
- ⁶⁶R. L. Puurunen, *Chem. Vapor Depos.*, **11**, 79–90 (2005).
- ⁶⁷T. Suntola, J. Antson, A. Pakkala, and S. Lindfors, “Atomic layer epitaxy for producing EL-thin films,” in *SID International Symposium. Digest of Technical Papers*, pp. 108–109 (1980).
- ⁶⁸S. I. Zaitso, S. Motokoshi, T. Jitsuno, M. Nakatsuka, and T. Yamanaka, *Japanese J. Appl. Physics, Part 1 Regul. Pap. Short Notes Rev. Pap.*, **41**, 160–165 (2002).
- ⁶⁹D. R. G. Mitchell, G. Triani, D. J. Attard, K. S. Finnie, P. J. Evans, C. J. Barbé, and J. R.

- Bartlett, *Smart Mater. Struct.*, **15**, S57–S64 (2006).
- ⁷⁰I. Jõgi, K. Kukli, M. Kemell, M. Ritala, and M. Leskelä, *J. Appl. Phys.*, **102**, 114114 (2007).
- ⁷¹M. Laitinen, T. Sajavaara, M. Rossi, J. Julin, R. L. Puurunen, T. Suni, T. Ishida, H. Fujita, K. Arstila, B. Brijs, and H. J. Whitlow, *Nucl. Instruments Methods Phys. Res. Sect. B Beam Interact. with Mater. Atoms*, **269**, 3021–3024 (2011).
- ⁷²V. Fedorenko, I. Iatsunskyi, M. Pavlenko, M. Jancelewicz, E. Coy, and R. Viter, *Proc. SPIE*, **9649**, 96490X (2015).
- ⁷³R. L. Puurunen, T. Sajavaara, E. Santala, V. Miikkulainen, T. Saukkonen, M. Laitinen, and M. Leskelä, *J. Nanosci. Nanotechnol.*, **11**, 8101–8107 (2011).
- ⁷⁴R. L. Puurunen, J. Kiihamäki, and H. Kattelus, *AVS Topical Conference on Atomic Layer Deposition, San Jose, California 8-10 August* (2005).
- ⁷⁵S. K. Kim, S. Hoffmann-Eifert, M. Reiners, and R. Waser, *J. Electrochem. Soc.*, **158**, D6–D9 (2011).
- ⁷⁶R. L. Puurunen and W. Vandervorst, *J. Appl. Phys.*, **96**, 7686 (2004).
- ⁷⁷V. S. Lusvardi, M. a Barteau, W. R. Dolinger, and W. E. Farneth, *J. Phys. Chem.*, **100**, 18183–18191 (1996).
- ⁷⁸G. D. Parfitt, “The Surface of Titanium Dioxide,” in *Progress in Surface and Membrane Science*, Volume 11., D. A. Cadenhead, Ed. Academic Press, (1976), pp. 181–226.
- ⁷⁹R. L. Puurunen, M. Lindblad, A. Root, and A. O. I. Krause, *Phys. Chem. Chem. Phys.*, **3**, 1093–1102 (2001).
- ⁸⁰M. F. Doerner and W. D. Nix, *CRC Crit. Rev. Solid State Mater. Sci.*, **14**, 225–268 (1988).
- ⁸¹T. O. Kääriäinen, P. J. Kelly, D. C. Cameron, B. Beake, H. Li, P. M. Barker, and C. F. Struller, *J. Vac. Sci. Technol. A*, **30**, 01A132 (2012).